CHARACTERISTIC OF CRYOGENIC HYDROGEN FLAMES FROM HIGH-ASPECT RATIO NOZZLES

Ethan S. Hecht[a], and Bikram Roy Chowdhury[a]

[a]Combustion Research Facility, Sandia National Laboratories, P.O. Box 969, MS 9052, Livermore, CA, 94551, USA, ehecht@sandia.gov, broycho@sandia.gov

ABSTRACT

Unintentional leaks at hydrogen fueling stations have the potential to form hydrogen jet flames, which pose a risk to people and infrastructure. The heat flux from these jet flames are often used to develop separation distances between hydrogen components and buildings, lot-lines, etc. The heat flux and visible flame length is well understood for releases from round nozzles, but real unintended releases would be expected to be be higher aspect-ratio cracks. In this work, we measured the visible flame length and heat-flux characteristics of cryogenic hydrogen flames from high-aspect ratio nozzles. We compare this data to flames of both cryogenic and compressed hydrogen from round nozzles. The aspect ratio of the release does not affect the flame length or heat flux significantly, for a given mass flow under the range of conditions studied. The engineering correlations presented in this work that enable the prediction of flame length and heat flux can be used to assess risk at hydrogen fueling stations with liquid hydrogen and develop science-based separation distances for these stations.

1.0 INTRODUCTION

A fuel cell electric vehicle can go approximately twice as far on 1 kg hydrogen as a gasoline vehicle can travel on 1 gallon of gasoline [1, 2]. One kg liquid hydrogen occupies approximately 14 l, and one gallon is 3.8 l. In other words, to propel the same number of vehicles the same distance, liquid hydrogen would occupy approximately 80% more volume than gasoline. Even at a storage pressure of 500 bar, the hydrogen at a fueling station would occupy 2.3 times more volume than liquid hydrogen (or over 4 times the volume of gasoline). For an equivalent delivery truck fuel volume, a compressed hydrogen tube trailer at the maximum delivery pressure of 250 bar (in the U.S.) would require 4 times as many deliveries as a liquid hydrogen truck. With these simple calculations, it becomes clear that in lieu of pipelines or on-site generation, liquid hydrogen is the medium of choice for fueling station delivery and on-site storage when thinking of replacing gasoline fueling infrastructure with hydrogen.

The California Fuel Cell Partnership projects that 1000 retail hydrogen stations need to be opened by 2030 to support up to one million vehicles in California [3]. The study illustrated that the fueling station density needs to be high in urban centers, including San Francisco, Los Angeles, and San Diego. This will require placing bulk liquid hydrogen storage in space-constrained sites. The minimum separation distances from bulk liquefied hydrogen storage to lot lines, air intakes and building openings as set by the current 2016 edition of National Fire Protection Agency Hydrogen Technologies Code (NFPA 2) [4] are in some cases more than twice as large as similar bulk gaseous hydrogen storage. Even with credits for insulation and fire-rated barrier walls, the 23 m separation distance to building openings/air intakes can be challenging to meet in urban areas. Safety for hydrogen infrastructure is of utmost importance,

but the current liquid hydrogen separation distances are based on subjective expert opinion rather than physical models, and thus may be overly conservative.

Several groups have investigated the ignition and flame characteristics of cryogenic hydrogen releases. Hall et al. [5] reported experimental studies of ignited liquid hydrogen releases with spill rates similar to a transfer hose operations. Based on the radiation heat flux measurements for the large spill rates (60 l/min) in this study, they formulated a safety distance around 11.5 m, less than half the value in NFPA 2. More detailed experiments have been performed in controlled laboratory settings by Friedrich et al. [6] and Panda & Hecht [7]. Friedrich et al. [6] studied horizontal cryogenic hydrogen flames with the various release temperatures (35–65 K), pressures (0.7–3.5 MPa), and nozzle diameters (0.5 and 1 mm). Ignition at a point in the jet led to three combustion regimes: 1) flash-back and a stable diffusion flame at the nozzle, 2) a stable distant burn without flasback, or 3) unstable transient burn with quenching. The measured radiation heat flux values were shown to be correlated to the hydrogen mass flow rate. Panda & Hecht [7] investigated cryogenic under-expanded hydrogen jet flames over a range of temperaturse (37–295 K), pressures (0.2–0.6 MPa) and nozzle release diameters (0.75–1.25 mm). The maximum ignition distance was found to be higher for colder, cryogenic releases at a fixed hydrogen mass flow rate, than for room temperature jets. The classical flame length models were shown to be valid for the tested flow conditions. For a fixed hydrogen mass flow, the radiative heat flux was reported to increase with decrease in release temperature which was attributed to lower choked flow velocity of colder hydrogen source which increased the flame residence time.

Realistic leak exit geometries are not likely to be circular, but rather cracks and slits with a high aspect ratio, or other complex geometries. Relative to diffusion flames resulting from circular nozzles, limited work has been done to develop correlations of flame length for slot flames or other complex geometries. Henriksen et al. [8] demonstrated that for a given mass flow rate, a larger orifice downstream of a choking orifice could increase the flame length by up to 62%, relative to a simple nozzle. Gollahalli et al. [9] found that an elliptical nozzle (aspect ratio of 3) enhanced entertainment, which resulted in accelerated destruction of the fuel species and a slightly lower radiation flux, although the lower flux was attributed to less soot in these propane flames. In an experimental study by Mogi & Horiguchi [10], hydrogen flame lengths from slit nozzles with aspect ratios of 5 and 12.8 were compared to that of a round nozzle with an identical cross-sectional area. They showed that for fixed release pressure, the flame length of a round nozzle was the longest while for slit nozzles, it decreased with increasing aspect ratio. Makarov & Molkov [11] have performed detailed numerical simulation to study the flow field for releases from axisymmetric and plane nozzles. The reacting simulation was in good agreement with the experimental results of Mogi & Horiguchi [10]. However, these works have been limited to room temperature releases and aspect ratio of 12.8. For development of safety codes and standards for deployment of liquid hydrogen infrastructure, it is important to validate these observations at relevant cryogenic temperatures and pressures.

2.0 EXPERIMENTAL

Cryogenic hydrogen flame experiments were performed at the Turbulent Combustion Laboratory at Sandia National Laboratories. The cryogenic hydrogen release platform as described in detail by Panda & Hecht [7] was used in this study. Briefly, a metered quantity of gaseous hydrogen at room temperature was cooled to cryogenic temperatures using a three-stage heat exchanger. The first stage of the heat exchanger cooled hydrogen to about 80 K using liquid nitrogen. The second stage utilized cold gaseous helium to further cool the hydrogen in a counter-flow tube-in-tube heat exchanger. Finally, the hydrogen was cooled to its saturation temperature by flowing it through a bath of liquid helium. The cryogenic hydrogen flowed into the laboratory

Table 1. Operating conditions during experiments.

Experimental Parameter	Range
pressure (bar_{abs})	1.5–6.0
temperature (K)	42–295
hydrogen mass flow rate (g/s)	0.054–0.544

Table 2. Nozzle dimensions.

aspect ratio label	length (mm)	width (mm)
round	1.0 (diameter)	
AR2	0.627	1.253
AR4	0.443	1.773
AR8	0.313	2.507
AR16	0.222	3.545
AR32	0.157	5.013
AR64	0.111	7.090

through a single vacuum jacketed line. Heat leaks in this line caused the hydrogen temperature to increase by the time it flowed to the release point.

The test conditions of the hydrogen jet flame experiments are summarized in Table 1. In addition to a 1 mm diameter round nozzle, six rectangular slot nozzles with aspect ratios of 2, 4, 8, 16, 32 and 64 were studied in this work. The length and width of each slot nozzle was set such that the exit area was equivalent to that of a 1 mm diameter circular nozzle, as shown in Table 2. The nozzles were machined via laser drilling and optical microscopy showed the accuracy of dimensions to be within 30 μm. Thermal expansion (or contraction due to the cryogenic conditions) is will not affect these dimensions significantly. For the lifted hydrogen flames, the thermal feedback to the nozzle is very limited.

To calculate the flame length and flame width, visible flame images were captured in a dark room by a commercial Panasonic Lumix camera at an f-stop of 2.8 using a 100 ms exposure time. The flame length was defined as the distance from the nozzle exit along the axis of the flame where the intensity drops to 10% of the maximum intensity level of that image.

Radiant heat flux is a key mechanism of heat transfer from flames and is an important property for safety codes and standards. The radiant heat flux was measured by five wide-angle Medtherm Model 64P-1-22 Schmidt-Boelter thermopile detectors, each with a 150° view angle. A Zn-Se window on the face of each radiometer has 70% transmission between 0.7 and 17 μm. The radiometers were installed at five different downstream distances (6.4, 22, 32, 42, and 65 cm) and radially 20 cm away from the jet axis, similar to Panda & Hecht [7] to compare the cryogenic hydrogen flames of circular and rectangular nozzles for a given mass flow rate.

3.0 RESULTS AND DISCUSSIONS

As discussed in Panda & Hecht [7], the mass flow rate of the hydrogen is measured as a gas upstream of the heat exchanger. The temperature is measured and the pressure is controlled just upstream of the nozzle. Through the CoolProp library [12] we used the real gas equation of state for hydrogen [13] to calculate the flow rate assuming isentropic expansion as the cryogenic gas flowed through the nozzle. This calculated flow rate, for a cross sectional area of a 1 mm

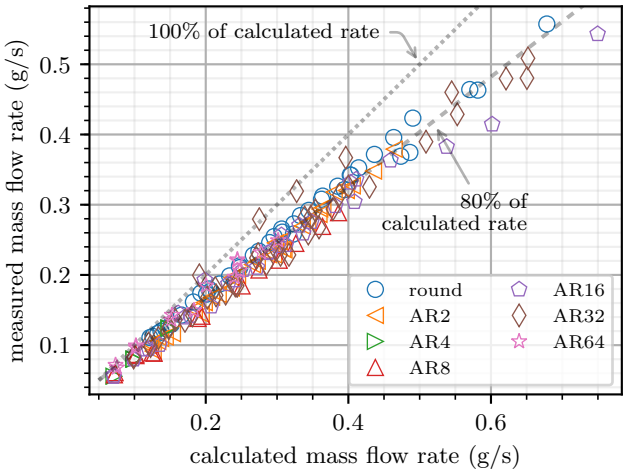

Figure 1. Measured mass flow rate vs calculated mass flow rate.

diameter nozzle is shown vs the measured flowrate (upstream of the heat exchanger) for all of the flames studied in Fig. 1. While there are a few measured mass flow rates are near or even slightly above the calculated mass flow rates, the majority of the measured mass flow rates are around 80% of the calculated rate. The higher measured mass flow rates may be due to noise on the mass flow measurements. The lower mean measured mass flow rate seems to be independent of the aspect ratio of the nozzle and is also true for the round nozzle. This indicates that the combination of nozzle losses and dimensional errors in machining for all of these nozzles can be accounted for by modeling the flow through a 1 mm round nozzle with a coefficient of discharge of 0.8.

3.1 Visible flame length

Flame length is an important property used in fire research that is often used to scale other aspects of flames. For development of science-based safety codes and standards, it is important to identify the worst-case scenario and use the worst-case as a conservative approach. The experimental work of Mogi and Horiguchi demonstrated that the hydrogen flame length was longer for a round nozzle than for slit nozzles [10]. This observation has been experimentally tested only for aspect ratios of 5 and 12.8 [10].

The visible flame lengths measured at various release pressure and temperature for the round nozzle as well as the six different aspect ratio nozzles are shown in Fig. 2, as a function of hydrogen mass flow rate. For all of the nozzles, it is clearly seen that there is an increase in flame length with hydrogen mass flow rate which follows the trend reported previously for round nozzles [7]. For a fixed mass flow rate, the flame length is observed to increase with a decrease in nozzle temperature, which was also observed previously [7]. The data for the round nozzles aligns well with all of the different aspect ratios studied in this work.

The mass flow rate of hydrogen is governed by the pressure and temperature of the releases. For slit nozzles, the effect of these two regulating parameters on visible flame length measurements is shown in Fig. 3. The nozzle temperature for the ignited releases is indicated by the color of the markers. As expected, the visible flame length increases with release pressure for a given nozzle temperature. A similar variation of flame length for slit nozzles have been shown by Mogi & Horiguchi [10]. For a fixed release pressure, the flame length decreases significantly with an increase in nozzle temperature, as was discussed in reference to Fig. 2, but can be seen clearly here by inspecting the flame lengths in the three different frames. This decrease

can be attributed to lower mass flow rates (due to the lower density) at higher temperatures. For example, at 5 bar_{abs} (for the AR32 case), increasing the temperature from 42 K to 240 K decreases the flame length by a factor of 3.5. The mass flow rate (with a coefficient of discharge of 0.8) for a 5 bar, 42 K and 240 K release are 0.46 and 0.22 g/s, receptively. This is a decrease by a factor slightly over 2, so the decreased mass flow rate is not solely responsible for the increase in flame length. As discussed in Panda & Hecht [7], lower temperatures result in lower choked flow velocities for cryogenic hydrogen jets. This can in turn decrease the entrainment of air thereby increasing the reaction zone and flame length at lower temperatures.

Figures 2 and 3 show that while there is some scatter in the data, the visible flame length does not appear to be dependent on the geometry of the release. For a given flow condition, the visible flame length is the same for the round nozzle as for all aspect ratios from 2-64. For some conditions, we see that the visible flame length for AR32 is higher than the other cases. This can be attributed to the uncertainties involved in estimating the visible flame length. However, the flame length measurements follow a general trend which shows negligible influence of aspect ratio for releases at similar temperature and pressure. The flame shapes for the high aspect ratio slot nozzles are also similar to those of the round nozzles. The width is approximately $0.17L_f$, similar to the round nozzles.

The lack of flame length dependence on aspect ratio is counter to the observation by Mogi and Horiguchi [10] who found the flame length to decrease significantly as the aspect ratio increased. Differences in experimental observations can at least partially be attributed to the experimental setups and definition of flame length. While we measured actual emissions from these hydrogen flames (emissions from radicals produced from the hydrogen/oxygen reaction), Mogi & Horiguchi [10] measured emission from sodium, from a Na_2CO_3 solution that was sprayed into the flames. The optical emissions from these two different methods will certainly not be in identical locations, and the sodium emission method may be more sensitive to minor temperature difference between the nozzle geometries. In addition, a plane hydrogen jet (or flame in this case) is often characterized by three regions: potential core, two-dimensional flow region, and an axisymmetric flow zone. The 'axis switch' phenomenon is associated with the two-dimensional flow region which provides faster mixing in the near field. A numerical study by Makarov and Molkov [11] has shown that pressure has direct impact on the axis switching: higher release pressures result in longer two-dimensional flow regions. In an additional work which has been submitted to this conference [14], we made concentration measurements on

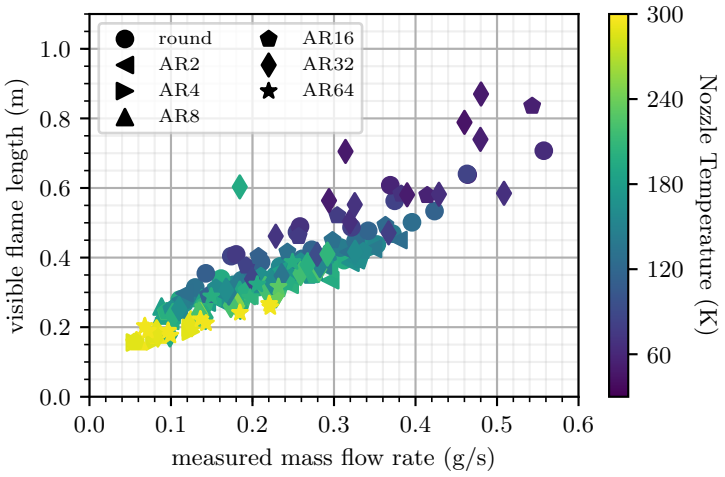

Figure 2. Flame length as a function of mass flow rate

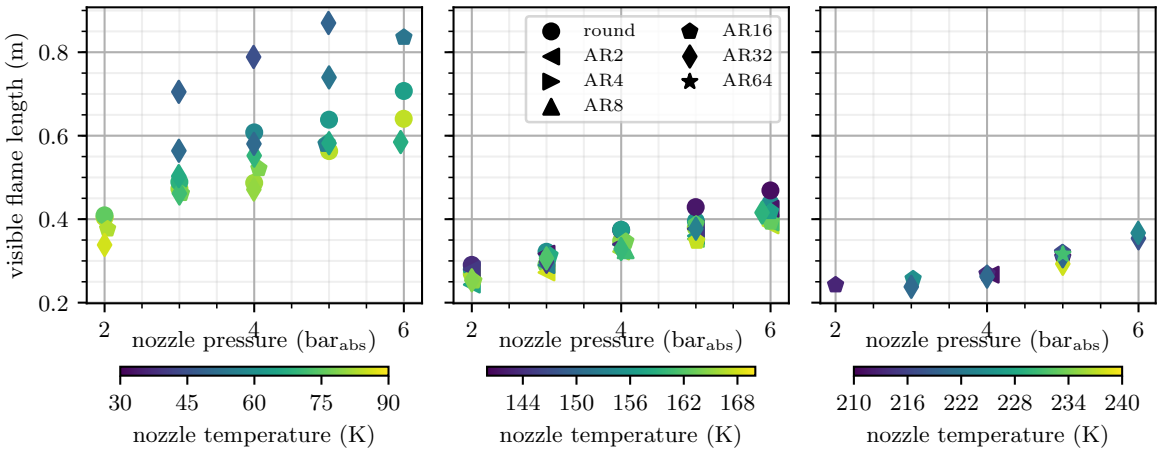

Figure 3. Flame length variation as a function of pressure for several binned temperatures.

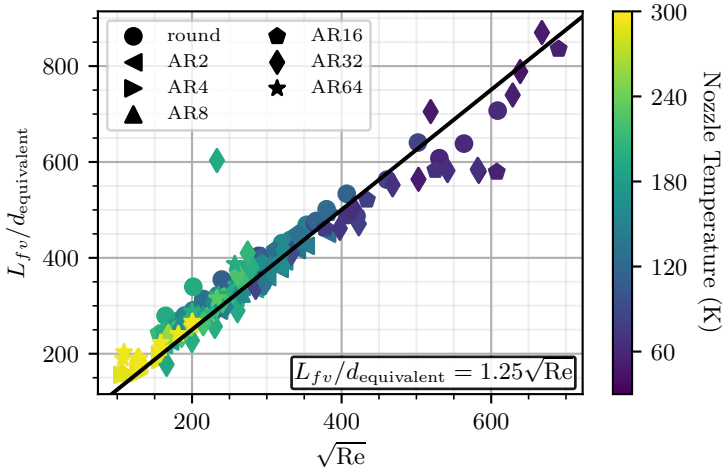

Figure 4. Normalized visible flame length as a function of the square root of the Reynolds number.

uniginited releases. These concentration measurements show that for low pressure cryogenic releases, the two-dimensional flow region is short and does not lead to enhanced mixing and a smaller flammable envelope which agrees with the flame length estimates reported here. The implication of this study, and the work of Mogi & Horiguchi [10] is that for assessing the safety of hydrogen systems, the assumption that the round nozzle has the longest flame length (or at worst an equivalent flame length) as a high aspect ratio crack or slit with the same flow area, is valid.

All of the visible flame length data is shown to collapse in Fig. 4. The flame length normalization was performed, similar to Panda & Hecht [7], by the diameter (in the case of the different aspect ratio nozzles, the equivalent diameter was specified as 1 mm, as this would be the diameter of a round nozzle with the same flow area), and it is plotted as a function of the square root of the Reynolds number. All of the normalized visible flame lengths are linear with respect to the square root of the Reynolds number, with a slope of 1.25. This slope is higher than that reported by Panda & Hecht [7], but there appears to be an error in the reported slope of 0.85 in the text; the slope of the line in the plot is 1.27 which is very close to the value in Fig. 4.

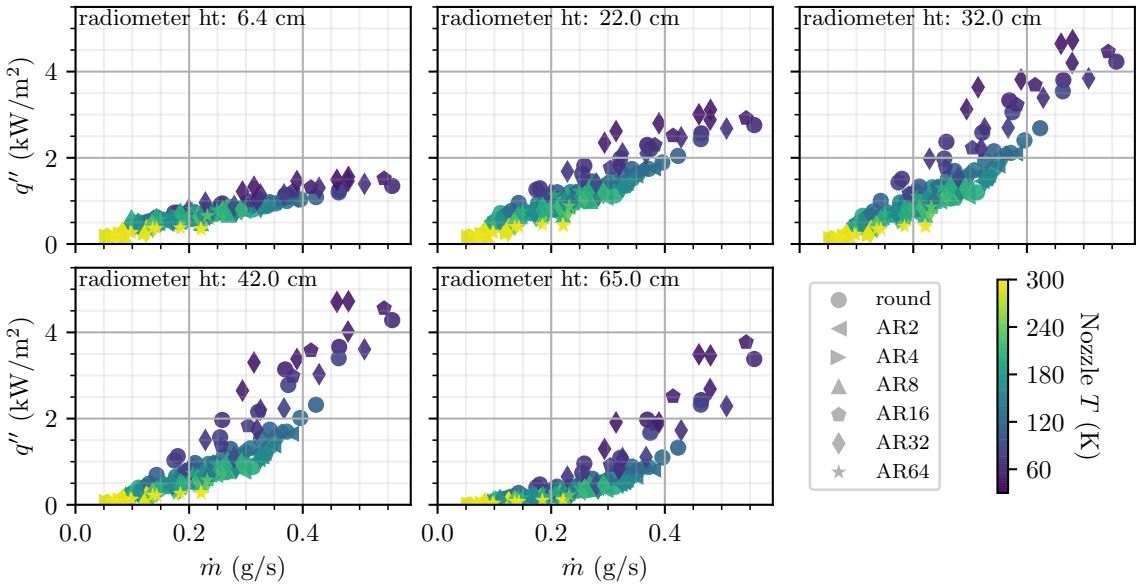

Figure 5. Radiative heat flux measured by each of the radiometers for all test conditions.

3.2 Radiation from the flame

Relative to traditional gaseous fuel flames (e.g. methane, propane – which contain carbon that tends to form soot particles), the radiant emission from hydrogen flames is smaller. However, the hazardous effect of thermal radiation on the surroundings cannot be ignored. The thermal radiation from the different slot nozzles at the tested conditions was measured with five radiometers at various heights above the nozzle. The variation of radiative heat flux measured by each of the radiometers as a function of hydrogen mass flow rate is shown in Fig. 5. As expected, there is an increase in heat flux with increase in hydrogen mass flow rate. Similar to the visible flame length, for a fixed mass flow rate of hydrogen, the radiative heat flux is higher for colder jet releases.

Because we have five radiometers measuring the same flame, assumptions made in classical radiant heat flux analyses can be explored. Sivanthu & Gore [15] suggest that the radiant energy leaving a flame can be calculated based on a single heat flux measurement located at 0.5–0.7 times the flame length. This is the approach adopted by Schefer et al. [16] as well as Panda & Hecht [7]. Hankinson & Lowesmith [17], on the other hand, suggest a weighted multi-source method for calculating the radiated energy from the flame. In these analyses, a quantity of interest is the radiant fraction, X_{rad}, which is the fraction of total chemical heat release that is radiated to the surroundings, or

$$X_{\text{rad}} = \frac{Q_{\text{rad}}}{\dot{m}_{\text{fuel}} \Delta H_c} \tag{1}$$

where Q_{rad} is energy radiantly emitted from the flame, $\dot{m}_{\text{fuel}}$ is the mass flow rate, ΔH_c is the heat of combustion. The product, $\dot{m}_{\text{fuel}} \cdot \Delta H_c$ is the total energy in the flame.

The heat flux sensors are measuring the heat flux emitted from the flame. The single point and weighted multi-source methods are different means for calculating Q_{rad} from heat flux measurements. In the case of the single-point method,

$$Q_{\text{rad}}^{\text{SP}} = q'' 4\pi S^2 \tag{2}$$

where S is the distance from the sensor to the point on the flame that is 0.5–0.7 times the flame length and q'' is the heat flux measured by the sensor. In other words, it is as if the flame is

radiating the heat from this single point on the flame. The most accurate measurement of the heat flux would be if the sensor is located at 0.5–0.7 times the flame length, but in theory, as long as S is the distance to this point on the flame, it should result in the same calculated radiated energy. Note that in this approach, we are assuming that the response of the radiometer is not dependent on the incident angle of the radiation. The weighted multi-source method, on the other hand, sums the contributions of the flame along its length. Rather than having a number of discrete points, we take the multi-source method one step further and consider the discretization to shrink to differential elements. In this case, a weighting function, w is used to characterize the amount of the radiant energy leaving flame at each differential element along its length, or

$$dQ_{\text{rad}}^{\text{WMP}} = wQ_{\text{rad}}^{\text{WMP}}dy, \tag{3}$$

where dy is a differential element along the flame. Therefore, the weighted multi-point radiant energy can be calculated as

$$Q_{\text{rad}}^{\text{WMP}} = q'' \Big/ \int_0^{L_f} \frac{w}{4\pi S^2} dy, \tag{4}$$

where both S and w are functions of y. We have once again assumed that the response of the radiometer is not dependent on the incident angle of the radiation, which differs from the analysis by Hankinson & Lowesmith [17]. We are also, in this treatment, ignoring the effect of atmospheric transmission losses due to the fact that our radiometers are less than 1 m from our flames. For large scale flames where the transmission distances are large, the transmissivity will need to be included in the analysis [17].

We used a weighting function similar to Hankinson & Lowesmith [17] in this analysis, where the weighting is zero at the nozzle and L_f, and climbs linearly to a maximum at some point along the flame length. In this case, $\int_0^{L_f} wdy = 1$ has been used to normalize the weighting function and it can be written as

$$\begin{cases} \frac{2y}{L_f^2 y_{\text{peak}}}; & 0 \le y \le y_{\text{peak}} \\ \frac{2(L_f - y)}{L_f^2(1-y_{\text{peak}})}; & y_{\text{peak}} < y \le L_f \end{cases}, \tag{5}$$

where y_{peak} is the point along the flame axis where the radiant heat flux is at a maximum. The radiant energy using the multi-point assumption (Eq. 4) is compared to the radiant energy calculated using the single-point method (Eq. 2) in Fig. 6. Due to our definition of visible flame length as the point where the intensity dropped to only 10% of the maximum, and the observation that IR flame lengths (which radiate heat collected by the sensors) are longer than visible flame lengths [7], we estimated the flame length for these calculations to be 30% larger than the visible flame lengths reported in the previous section. The flame centroid was assumed to be 0.5 times the flame length (or 0.65 times the visible flame length) for the single-point method, and the peak weighting was specified as 0.5 times the flame length for the multi-point method. As shown, when the sensor is downstream of the flame length, both the single-point and multi-point calculations are within 5% of each other. The single-point calculation gives the lowest radiant energy calculation, relative to the multi-point calculation at approximately 0.5 times the flame length, at approximately 70% of the multi-point calculation. For a sensor that is near the nozzle exit, the single-point calculation will give a radiant energy that is higher than the multi-point calculation. Sivanthu & Gore [15] found that a single-point calculation of the total radiant output of the flame from a sensor at 0.5–0.7 times the flame length could be made with a C^* value (a non-dimensional parameter $C^* = q''4\pi S^2/(\dot{m}_{\text{fuel}}\Delta H_c X_{\text{rad}})$ of 0.85. When y_{sensor} is 0.5–0.7 times the flame length, the single-point measurement of heat flux varies from around 0.7–1.0, with an average around 0.85 times the multi-point radiant energy.

The calculated mean radiant fraction (mean of the five radiometers) using the multi-point and single-point modes are shown in Fig. 7. This figure also shows the standard deviation of

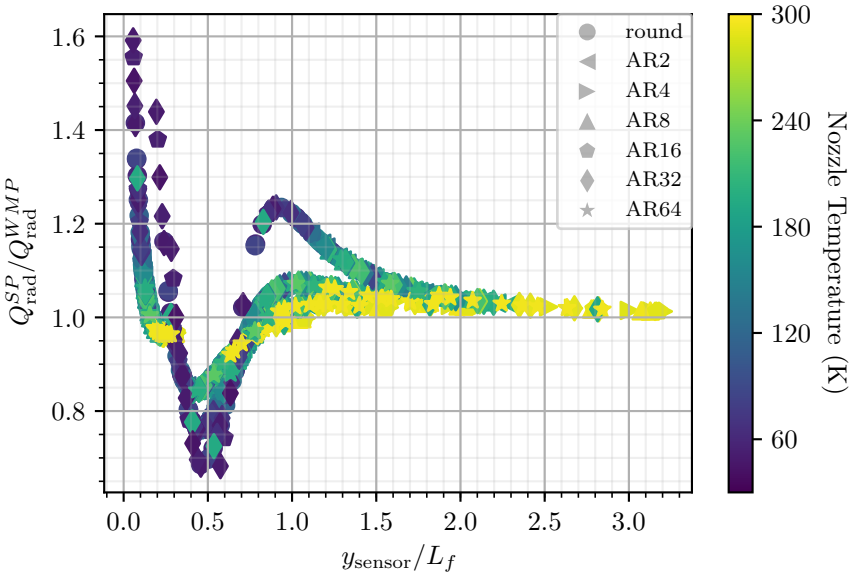

Figure 6. Relative radiant energy calculation using the single-point vs the multi-point method, for all of the five radiometers in this study, as a function of the normalized sensor distance along the flame axis.

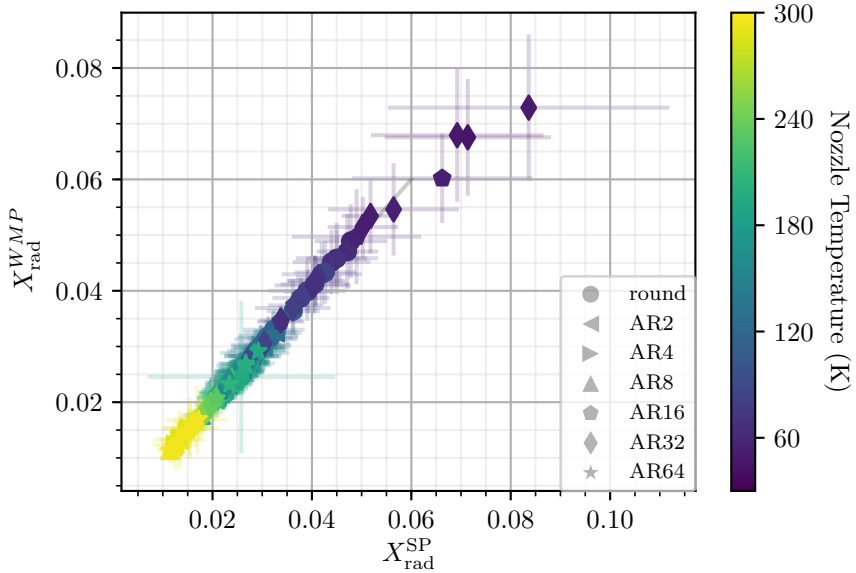

Figure 7. Mean radiant fraction (from all 5 radiometers) calculated using the multi-point vs the single-point method. Errorbars (shown as faint lines in each direction) are the standard deviation of the calculations from the 5 radiometers.

the 5 radiometers as errorbars on each of the points. The deviation of the 5 radiometer for calculating the radiant fraction is about twice as large for the single-point calculations than for the multi-point method. This highlights that radiometer placement is critical for a single-point measurement of radiant energy. Using all 5 radiometers, the methods result in very similar mean radiant fractions. At low temperature with high radiant fraction, the mean single-point radiant fractions are slightly higher than the mean multi-point radiant fractions.

Radiant fraction has been demonstrated to be a function of the flame residence time [7, 18]. The radiant fraction from the flames of cryogenic hdrogen from the different aspect ratio nozzles are compared to the round cryogenic jets, as well as other fuels in Fig. 8. The radiant fractions, calculated using the multi-point calculations for the radiant energy align well with the previous data for round cryogenic hydrogen jets as well as some literature data for methane flames. Once again, this plot shows that all of the hydrogen flames have a lower radiant fraction than methane flames, and that the radiant fraction and residence times increase for the colder release conditions than the warmer release conditions. The power-law fit captures the trend from the cryogenic hydrogen data as well as the literature values for the methane flames. The data fit is

$$X_{\text{rad}} = 2.33 \times 10^{-8} (\tau_g a_P T_f^4)^{0.44}, \tag{6}$$

where tau_g is the global residence time, a_P is the Plank mean absorption coefficient, and T_f is the adiabatic flame temperature for the fuel, as described in the literature [7, 18]. This correlation can be used to assess the radiant fraction for cryogenic hydrogen flames (as well as warm hydrogen flames and other fuels), which can in turn be used to calculate the radiant heat flux for safety assessments.

4.0 SUMMARY AND CONCLUSIONS

For the safe deployment of hydrogen based technologies, understanding the flame characteristics and radiative heat flux from a turbulent jet flame release which can arise from an accidental leakage in a hydrogen storage system is of paramount importance. Conventionally, the releases from round nozzles have been considered as worst-case scenario based on prior research which were limited to room temperature releases and low aspect ratio. In this work, cryogenic hydrogen

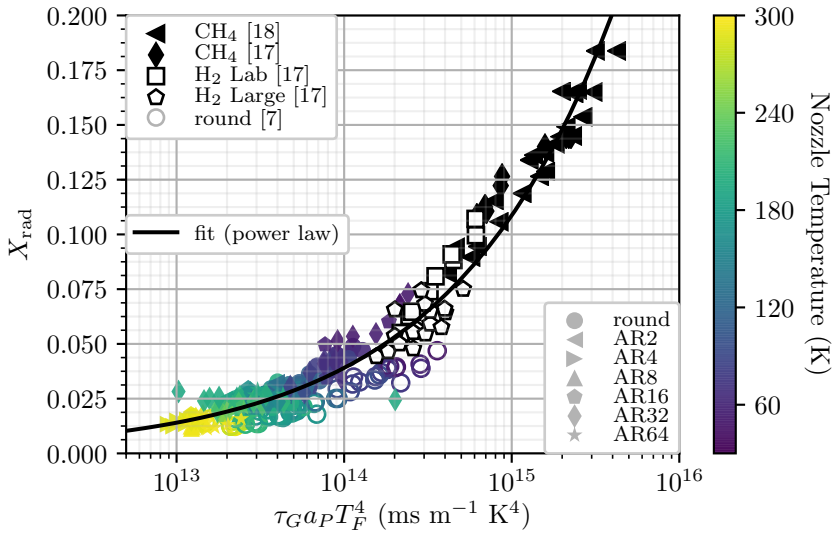

Figure 8. Radiant fraction for cryogenic hydrogen and other literature values for other fuels.

jet flames were investigated over a range of temperatures (42—295 K), pressures (0.5—6 bar) and aspect ratios (2–64).

As with flames from round release geometries, visible flame length and radiative heat flux increased with mass flow rate. For slit nozzles at identical hydrogen flow rates, the aspect ratio did not significantly affect the visible flame length or width. A correlation was shown that linearly scales the flame length with the square root of the Reynolds number. This correlation is valid for either round or high aspect ratio releases.

Heat flux measurements from 5 radiometers were used to assess the single-point vs the multi-point methods for interpretation of heat flux sensor data. The single-point calculations of radiant energy varied relative to the multi-point calculation, based on the axial placement of the sensor. Nonetheless, the average radiant energy calculation for the five sensors was similar, regardless of the flame conditions. The aspect ratio did not significantly affect the radiant fraction for these cryogenic hydrogen flames. A power law fit was used to relate the radiant fraction to the flame residence time, which is valid for cryogenic hydrogen through round nozzles, high aspect ratio nozzles, as well as other fuels.

This work shows that assuming a round nozzle release geometry will not significantly affect visible flame length or radiant heat flux calculations, and presents updated correlations for calculating these parameters.

5.0 ACKNOWLEDGMENTS

The U.S. Department of Energy's (DOE) office of Energy Efficiency and Renewable Energy's (EERE) Fuel Cell Technologies Office (FCTO) supports the development of science-based codes and standards through the Safety, Codes and Standards program sub-element. The authors gratefully acknowledge funding from FCTO and the support of subprogram manager Laura Hill for this work. Sandia National Laboratories is a multi-mission laboratory managed and operated by National Technology and Engineering Solutions of Sandia LLC, a wholly owned subsidiary of Honeywell International Inc. for the U.S. Department of Energy's National Nuclear Security Administration under contract DE-NA0003525. This paper describes objective technical results and analysis. Any subjective views or opinions that might be expressed in the paper do not necessarily represent the views of the U.S. Department of Energy or the United States Government.

REFERENCES

[1] National Renewable Energy Laboratory, NREL CDP: average on-road vehicle fuel economy (2017). URL https://www.nrel.gov/hydrogen/assets/images/cdp_fcev_114.jpg

[2] D.-Y. Lee, A. Elgowainy, A. Kotz, R. Vijayagopal, J. Marcinkoski, Life-cycle implications of hydrogen fuel cell electric vehicle technology for medium- and heavy-duty trucks, Journal of Power Sources 393 (2018) 217 – 229.

[3] California Fuel Cell Partnership, The california fuel cell revolution (Jul. 2018). URL https://cafcp.org/sites/default/files/CAFCR.pdf

[4] National Fire Protection Agency, NFPA 2: Hydrogen Technologies Code (2016).

[5] J. E. Hall, P. Hooker, D. Willoughby, Ignited releases of liquid hydrogen: Safety considerations of thermal and overpressure effects, Int. J. Hydrogen Energy 39 (35) (2014) 20547–20553.

[6] A. Friedrich, W. Breitung, G. Stern, A. Veser, M. Kuznetsov, G. Fast, B. Oechsler, N. Kotchourko, T. Jordan, J. Travis, J. Xiao, M. Schwall, M. Rottenecker, Ignition and heat radiation of cryogenic hydrogen jets, Int. J. Hydrogen Energy 37 (22) (2012) 17589–17598.

[7] P. P. Panda, E. S. Hecht, Ignition and flame characteristics of cryogenic hydrogen releases, Int. J. Hydrogen Energy 42 (1) (2017) 775–785.

[8] M. Henriksen, A. Gaathaug, J. Lundberg, Determination of underexpanded hydrogen jet flame length with a complex nozzle geometry, International Journal of Hydrogen Energy 44 (17) (2019) 8988 – 8996, special issue on The 7th International Conference on Hydrogen Safety (ICHS 2017), 11-13 September 2017, Hamburg, Germany.
[9] S. R. Gollahalli, T. Khanna, N. Prabhu, Diffusion flames of gas jets issued from circular and elliptic nozzles, Combustion Science and Technology 86 (1-6) (1992) 267–288.
[10] T. Mogi, S. Horiguchi, Experimental study on the hazards of high-pressure hydrogen jet diffusion flames, Journal of Loss Prevention in the Process Industries 22 (1) (2009) 45–51.
[11] D. Makarov, V. Molkov, Plane hydrogen jets, International Journal of Hydrogen Energy 38 (19) (2013) 8068–8083.
[12] I. H. Bell, J. Wronski, S. Quoilin, V. Lemort, Pure and pseudo-pure fluid thermophysical property evaluation and the open-source thermophysical property library coolprop, Ind. Eng. Chem. Res. 53 (2014) 2498–2508.
[13] J. W. Leachman, R. T. Jacobsen, S. G. Penoncello, E. W. Lemmon, Fundamental Equations of State for Parahydrogen, Normal Hydrogen, and Orthohydrogen, J. Phys. Chem. Ref. Data 38 (3) (2009) 721.
[14] B. Roy Chowdhury, E. S. Hecht, Dispersion of cryogenic hydrogen through high-aspect ratio nozzles, in: Proceedings of the International Conference on Hydrogen Safety, Adelaide, Austrailia, September 24-26, 2019.
[15] Y. Sivathanu, J. Gore, Total radiative heat loss in jet flames from single point radiative flux measurements, Combustion and Flame 94 (3) (1993) 265 – 270.
[16] R. Schefer, W. Houf, B. Bourne, J. Colton, Spatial and radiative properties of an open-flame hydrogen plume, International Journal of Hydrogen Energy 31 (10) (2006) 1332 – 1340.
[17] G. Hankinson, B. J. Lowesmith, A consideration of methods of determining the radiative characteristics of jet fires, Combustion and Flame 159 (3) (2012) 1165 – 1177.
[18] A. Molina, R. W. Schefer, W. G. Houf, Radiative fraction and optical thickness in large-scale hydrogen-jet fires, Proceedings of the Combustion Institute 31 (2) (2007) 2565 – 2572.
[19] S. R. Turns, F. H. Myhr, Oxides of nitrogen emissions from turbulent jet flames: Part i—fuel effects and flame radiation, Combustion and Flame 87 (3) (1991) 319 – 335.